CHINESE JOURNAL OF MECHANICAL ENGINEERING
Vol. 29, No. 3, 2016

DOI: 10.3901/CJME.2016.0314.031, available online at www.springerlink.com; www.cjmenet.com

Direct Yaw Moment Control for Distributed Drive Electric Vehicle Handling Performance Improvement

YU Zhuoping[1], LENG Bo[1], XIONG Lu[1,*], FENG Yuan[2], and SHI Fenmiao[1]

1 *School of Automotive Studies, Tongji University, Shanghai 201804, China*
2 *Pan Asia Technical Automotive Center Co., Ltd., Shanghai 201201, China*

Received June 7, 2015; revised August 10, 2015; accepted March 14, 2016

Abstract: For a distributed drive electric vehicle (DDEV) driven by four in-wheel motors, advanced vehicle dynamic control methods can be realized easily because motors can be controlled independently, quickly and precisely. And direct yaw-moment control (DYC) has been widely studied and applied to vehicle stability control. Good vehicle handling performance: quick yaw rate transient response, small overshoot, high steady yaw rate gain, etc, is required by drivers under normal conditions, which is less concerned, however. Based on the hierarchical control methodology, a novel control system using direct yaw moment control for improving handling performance of a distributed drive electric vehicle especially under normal driving conditions has been proposed. The upper-loop control system consists of two parts: a state feedback controller, which aims to realize the ideal transient response of yaw rate, with a vehicle sideslip angle observer; and a steering wheel angle feedforward controller designed to achieve a desired yaw rate steady gain. Under the restriction of the effect of poles and zeros in the closed-loop transfer function on the system response and the capacity of in-wheel motors, the integrated time and absolute error (ITAE) function is utilized as the cost function in the optimal control to calculate the ideal eigen frequency and damper coefficient of the system and obtain optimal feedback matrix and feedforward matrix. Simulations and experiments with a DDEV under multiple maneuvers are carried out and show the effectiveness of the proposed method: yaw rate rising time is reduced, steady yaw rate gain is increased, vehicle steering characteristic is close to neutral steer and drivers burdens are also reduced. The control system improves vehicle handling performance under normal conditions in both transient and steady response. State feedback control instead of model following control is introduced in the control system so that the sense of control intervention to drivers is relieved.

Keywords: direct yaw moment control, distributed drive electric vehicle, handling performance improvement, state feedback control

1 Introduction

Recently the direct yaw-moment control (DYC) has been widely applied in order to improve vehicle handling performance and stability[1]. For conventional internal combustion engine drive vehicles (ICVs) equipped with anti-lock braking system (ABS) and traction control system (TCS), DYC is usually realized by applying different braking force to wheels. But the brake system based DYC deteriorates acceleration[2] and the hydraulic unit cannot respond very fast. Compared to an ICV, a distributed drive electric vehicle (DDEV), which is driven by four in-wheel motors, has advantages not only in environmental protection but also in DYC[3]: Driving or braking torque on each wheel can be controlled independently, more quickly, and more precisely. Additionally, torque and speed information of the in-wheel motor can be obtained easily. Furthermore, based on DDEV the range of DYC is expanded, which makes the road adhesion utilization of four tires better balanced and extends the vehicle stability margin[4]; meanwhile, the DDEV-based DYC will not cause a strong sense of intervention to drivers and is more energy efficient[5].

In a variety of research on DDEV, DYC has focused on vehicle stability control under critical conditions[6–9], e.g. low adhesion road, high speed and large lateral acceleration. HE and his group proposed a hierarchical control methodology for stability improvement of 4WD EV in critical driving conditions[10]. The upper controller was based on the model following control (MFC) method and the lower controller distributes driving/braking force to each in-wheel motor to minimize tire utilization according to the generalized force calculated by the upper controller. Motoki Shino and Masao Nagai researched direct yaw moment control distribution methods to improve handling and stability of electric vehicles, in which a model following controller was also used as an upper controller[11–12]. In Ref. [13], an adaptive direct yaw moment control method based on identification of yaw rate model was proposed so that electric vehicles can track the desired dynamic model. Existing DYC research pays less attention to normal driving conditions. However, according

* Corresponding author. E-mail: xiong_lu@tongji.edu.cn
Supported by National Basic Research Program of China (973 Program, Grant No. 2011CB711200), National Science and Technology Support Program of China (Grant No. 2015BAG17B00), and National Natural Science Foundation of China (Grant No. 51475333)

to statistical results from Germany[14], the lateral acceleration on a good friction road is less than 4 m/s^2 in 95% of cornering driving conditions. Namely, vehicles work mostly under normal conditions where good handling performance is more urgently required by drivers: Vehicle yaw rate responses to the steering wheel input quickly with small overshoot; steering characteristics stay close to neutral steer even in high speeds and acceleration. Normally, the adhesion condition of the front axle is worse than the rear axle, which means the front axle gets into a non-linear region more easily and leads to bad maneuverability. Under normal conditions, tires stay in a linear region, and the vehicle system can be regarded as a linear system. According to the modern control theory[15], closed-loop poles and zeros in the controllable linear system can be placed at random through state feedback control to improve dynamic performance and stability margin.

This paper relies on the linear vehicle model by using the direct yaw moment control to improve the handling performance of a distributed drive electric vehicle equipped with four in-wheel motors especially under normal driving conditions. The designed controller consists of two parts: a state feedback controller, which aims to improve yaw rate transient response; and a steering wheel angle feedforward controller to achieve desired yaw rate steady gain because the state feedback will decrease the gain of steady-state yaw rate[16]. The integrated time and absolute error (ITAE) function[17] was utilized as the cost function in the optimal control to calculate optimum feedback matrix and feedforward matrix to assign ideal poles and zeros and to obtain enough steady gain of yaw rate. A state estimator based on the extended Kalman filter was adopted to obtain vehicle sideslip angle.

The allocation module is responsible for distributing the generalized force calculated by the upper controller to the actuators, i.e., the four independent in-wheel motors, on the premise that the driver's intention is satisfied.

2 Distributed Drive Electric Vehicle

A high performance distributed drive electric vehicle platform developed by Tongji University shown in Fig. 1(a) is equipped with a storage battery as the power source and four independent in-wheel motors. The main parameters of the DDEV are shown in Table 1 and the measurement system is shown in Fig. 1(b).

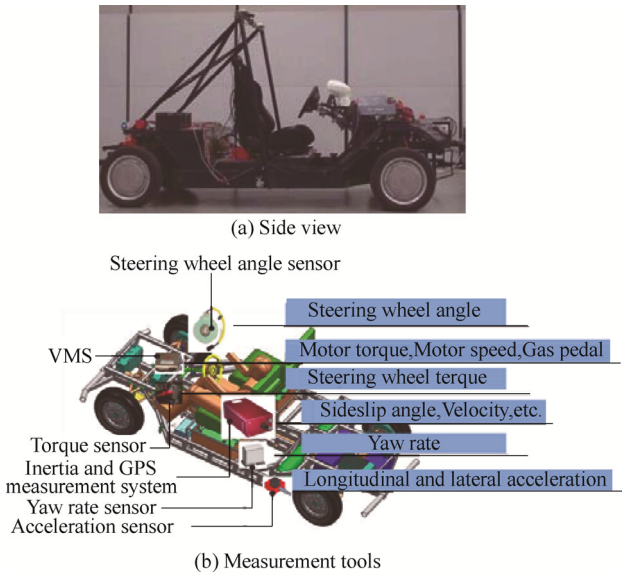

(a) Side view

(b) Measurement tools

Fig. 1. Distributed drive electric vehicle

Table 1. DDEV main parameters

Parameter	Value
Front axle to CG l_f/mm	1167
Rear axle to CG l_r/mm	1233
Wheel base l/mm	2400
Wheel track B/mm	1416
Rolling radius r/mm	292
Vehicle mass m/kg	1022
Yaw moment of inertia I_z/(kg • m^2)	1470
Steering system ratio	17.5
Peak power (one motor) P/kW	7.5
Peak torque (one motor) T/(N • m)	167

Note: CG means the center of gravity

3 Control System Structure

The designed controller is distinguished by the dotted line shown in Fig. 2. State feedback can compensate the error caused by external disturbance or model uncertainty. A full dimension state feedback controller was adopted to assign poles and zeros arbitrarily, namely, both of the vehicle sideslip angle β and the yaw rate $\dot{\psi}$ are fed back. However, feedback reduces system steady gain and steering sensitivity and results in worse handling performance. To solve this problem, a steering wheel angle feedforward controller was designed.

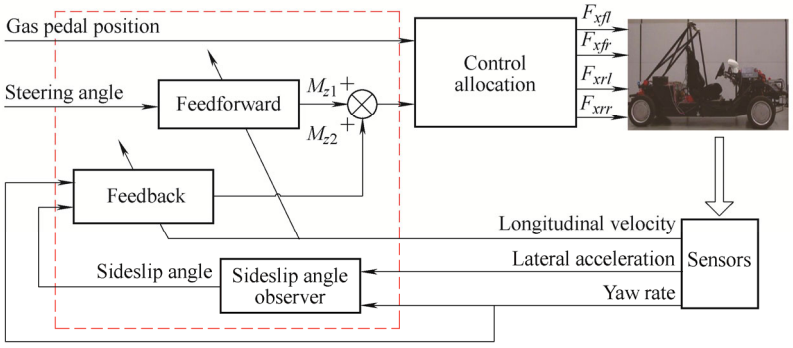

Fig. 2. Control system structure

The allocation module is responsible for distributing the generalized force calculated by the upper controller and demanded by the driver to the four independent in-wheel motors.

The sideslip angle of the vehicle is an important state variable to the controller. But it is hard to be measured directly and a sideslip angle sensor is too expensive to be employed in ordinary cars. Therefore, an estimator is adopted. Simulation results show the accuracy of the sideslip angle observer under normal conditions and prove that it meets control requirements.

4 Control System Design

4.1 Linear vehicle model

In order to make the control system design convenient and to reflect the main characteristics of vehicle handling, we make some ideal assumptions about the vehicle system.

(1) Drive on a flat road, no vertical road roughness input. Ignore vertical forces influence and coupling effects related to ride dynamics.

(2) Ignore suspension system; hence, load transfer and suspension dynamics are not taken into consideration.

(3) Steering system is rigid, and the transmission ratio between steering wheel and front wheels is constant.

(4) Ignore air resistance.

(5) Assure minimal disturbance of vehicle when it is near balance state. The lateral acceleration should be small (less than 0.4*g* on high friction road). Tires work in linear region, which means the lateral tire force merely increases proportionally as tire slip angle increases.

(6) The longitudinal velocity is constant.

Based on those assumptions, the vehicle is simplified to a typical two degrees of freedom model (2DOF model) as shown in Fig. 3.

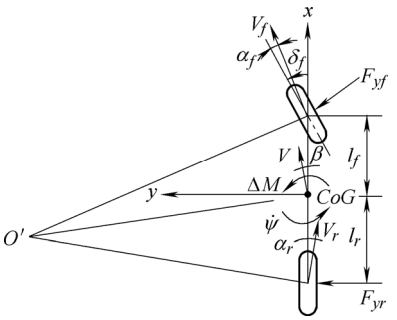

Fig. 3. 2DOF vehicle model

Only vehicle sideslip angle and yaw rate are taken into account as state variables. According to existing vehicle dynamics research[3, 9], this kind of simplification is reasonable and effective. In this paper, the 2DOF model is the fundamental model for control system design.

Newton's laws of motion are used to establish vehicle dynamic equations of plane motion. With reference to Fig. 3 forces along *y* axis and torques acting on the center of gravity are described as

$$\begin{cases} \sum F_y = F_{yf}\cos\delta_f + F_{yr}, \\ \sum M_z = l_f F_{yf}\cos\delta_f - l_r F_{yr}, \end{cases} \tag{1}$$

where δ_f is the steering angle of front wheels and is small, namely $\cos\delta_f \approx 1$. F_{yf} and F_{yr} are equivalent lateral forces on front axle and rear axle respectively, equal to the product of tire cornering stiffness and tire slip angle. The equivalent tire slip angles of front and rear axle can be calculated as follows:

$$\begin{cases} \alpha_f = \beta + \dfrac{l_f\dot{\psi}}{V} - \delta_f, \\ \alpha_r = \beta - \dfrac{l_r\dot{\psi}}{V}. \end{cases}$$

Eq. (1) can be written as

$$\begin{cases} \sum F_y = -C_f\left(\beta + \dfrac{l_f\dot{\psi}}{V} - \delta_f\right) - C_r\left(\beta - \dfrac{l_r\dot{\psi}}{V}\right), \\ \sum M_z = -l_f C_f\left(\beta + \dfrac{l_f\dot{\psi}}{V} - \delta_f\right) + l_r C_r\left(\beta - \dfrac{l_r\dot{\psi}}{V}\right), \end{cases} \tag{2}$$

where β —Vehicle sideslip angle, rad;
$\dot{\psi}$ —Yaw rate, rad/s;
V —Longitudinal velocity, m/s;
l_f, l_r —Distance from front/rear axle to CG, m;
C_f, C_r —Equivalent tire cornering stiffness of front/rear axle, positive, N/rad.

Furthermore,

$$\begin{cases} \sum F_y = ma_y, \\ \sum M_z = I_z\ddot{\psi}, \end{cases} \tag{3}$$

where I_z is the moment of inertia in yaw motion, $\mathrm{kg \cdot m^2}$; $\ddot{\psi}$ is yaw acceleration, $\mathrm{rad \cdot s^{-2}}$. The vehicle lateral acceleration $a_y = \dot{U} + V\dot{\psi}$, $\mathrm{m \cdot s^{-2}}$, in which U denotes lateral speed of CG and $U = \beta V$. So

$$a_y = (\dot{\beta} + \dot{\psi})V. \tag{4}$$

By combining Eqs. (2)–(4), the differential equation of 2DOF vehicle motion are obtained as follows:

$$\begin{cases} -(C_f + C_r)\beta + \dfrac{1}{V}(-l_f C_f + l_r C_r)\dot{\psi} + \\ \quad C_f\delta_f = mV(\dot{\beta} + \dot{\psi}), \\ (-l_f C_f + l_r C_r)\beta + \dfrac{1}{V}(-l_f^2 C_f + l_r^2 C_r)\dot{\psi} + \\ \quad l_f C_f\delta_f = I_z\ddot{\psi}. \end{cases} \tag{5}$$

The state space can be written as

$$\begin{cases}\dot{\boldsymbol{x}} = \boldsymbol{A} \bullet \boldsymbol{x} + \boldsymbol{B} \bullet \delta_f, \\ y = \boldsymbol{C} \bullet \boldsymbol{x}, \end{cases} \tag{6}$$

where state variable $\boldsymbol{x} = [\beta \quad \dot{\psi}]^{\mathrm{T}}$, output $y = \dot{\psi}$, system-matrix

$$\boldsymbol{A} = \begin{bmatrix} -\dfrac{(C_f + C_r)}{mV} & -1 - \dfrac{(C_f l_f - C_r l_r)}{mV^2} \\ -\dfrac{(C_f l_f - C_r l_r)}{I_z} & -\dfrac{(C_f l_f^2 + C_r l_r^2)}{I_z V} \end{bmatrix},$$

and control matrix

$$\boldsymbol{B} = \begin{bmatrix} \dfrac{C_f}{mV} \\ \dfrac{C_f l_f}{I_z} \end{bmatrix}.$$

Under normal conditions, the vehicle lateral acceleration is no more than 0.4*g* and the equivalent cornering stiffness C_f and C_r can be regarded as constant[14]. It is easy to get

$$\text{rank}[\boldsymbol{B}, \boldsymbol{AB}] = 2.$$

The original system is controllable.

Add extra yaw moment $\boldsymbol{M}_z$. The original state space Eq. (6) can be rewritten as

$$\begin{cases}\dot{\boldsymbol{x}} = \boldsymbol{A} \bullet \boldsymbol{x} + \boldsymbol{B} \bullet \delta_f + \dfrac{1}{I_z} \bullet \boldsymbol{M}_z, \\ y = \boldsymbol{C} \bullet \boldsymbol{x}. \end{cases} \tag{7}$$

4.2 Control strategy

Effects caused by poles and zeros to the system shown in Eq. (7) are considered simultaneously in this paper. In the control strategy, state feedback control is introduced to assign ideal poles, and yaw rate steady gain is ensured by a steering wheel angle feedforward controller.

The extra yaw moment $\boldsymbol{M}_z$ can be described in two parts shown in Eq. (8):

$$\begin{aligned} \boldsymbol{M}_z &= I_z \boldsymbol{Q} \boldsymbol{x} + I_z \boldsymbol{P} u, \\ \boldsymbol{M}_z &= \begin{bmatrix} 0 & 0 \\ I_z Q_1 & I_z Q_2 \end{bmatrix} \bullet \begin{bmatrix} \beta \\ \dot{\psi} \end{bmatrix} + \begin{bmatrix} 0 \\ I_z p \end{bmatrix} \bullet \delta_f. \end{aligned} \tag{8}$$

The feedback matrix can be obtained from Eq. (8):

$$I_z \boldsymbol{Q} = \begin{bmatrix} 0 & 0 \\ I_z Q_1 & I_z Q_2 \end{bmatrix}. \tag{9}$$

And the feedforward matrix is

$$I_z \boldsymbol{P} = \begin{bmatrix} 0 \\ I_z p \end{bmatrix}. \tag{10}$$

4.2.1 Feedback matrix

The system shown in Eq. (7) can be described as

$$\begin{cases}\dot{\boldsymbol{x}} = (\boldsymbol{A} + \boldsymbol{Q}) \bullet \boldsymbol{x} + (\boldsymbol{B} + \boldsymbol{P}) \bullet \delta_f, \\ y = \boldsymbol{C} \bullet \boldsymbol{x}. \end{cases} \tag{11}$$

The characteristic equation of the system matrix is

$$\begin{vmatrix} s - a_{11} & -a_{12} \\ -(a_{21} + Q_1) & s - (a_{22} + Q_2) \end{vmatrix} = s^2 - (a_{11} + a_{22} + Q_2)s + a_{11}(a_{22} + Q_2) - a_{12}(a_{21} + Q_1) = 0 \tag{12}$$

Poles of the ideal system are

$$s_{1,2} = -\omega_n \zeta \pm \omega_n \sqrt{1 - \zeta^2} \bullet j. \tag{13}$$

Combine Eqs. (12) and (13), get

$$Q_1 = -\frac{a_{11}(a_{11} + 2\omega_n \zeta) + {\omega_n}^2}{a_{12}} - a_{21}, \tag{14}$$

$$Q_2 = -2\omega_n \zeta - a_{11} - a_{22}. \tag{15}$$

By substituting Q_1 and Q_2 in Eq. (9), the feedback matrix can be obtained.

Eqs. (14) and (15) indicate that the feedback matrix is determined by parameters of the original system, ideal eigen frequency and damper coefficient.

4.2.2 Feedforward matrix

In the controlled system, the transfer function describing the relationship between the yaw rate and the steering angle is obtained by substituting Eq. (8) in the state space Eq. (6):

$$G_{\delta_f}^{\dot{\psi}}(s)' = \frac{b_1(a_{21} + Q_1) - a_{11}(b_2 + p)}{{\omega_n}^2} \bullet \frac{1 + T_s s}{1 + \dfrac{2\zeta}{\omega_n} s + \dfrac{1}{{\omega_n}^2} s^2}, \tag{16}$$

where

$$T_s = \frac{b_2 + p}{b_1(a_{21} + Q_1) - a_{11}(b_2 + p)},$$

and the gain matrix of the controlled system is

$$K = \frac{b_1(a_{21} + Q_1) - a_{11}(b_2 + p)}{{\omega_n}^2}.$$

If *K* is known (*K* is calculated in section 4.2.3), we can get

$$p=\frac{b_1(a_{21}+Q_1)-{\omega_n}^2K}{a_{11}}-b_2=$$
$$-\frac{{\omega_n}^2K+b_1\bullet\dfrac{a_{11}(a_{11}+2\omega_n\zeta)+{\omega_n}^2}{a_{12}}}{a_{11}}-b_2. \tag{17}$$

Zeros of the controlled are

$$s=-\frac{b_1(a_{21}+Q_1)}{b_2+p}+a_{11}=f(\omega_n,\zeta,K). \tag{18}$$

By substituting Eq. (17) in Eq. (10), the feedforward matrix is obtained as

$$I_z\boldsymbol{P}=I_z\begin{bmatrix}0\\p\end{bmatrix}=$$
$$\begin{bmatrix}0\\ I_z\left(-\dfrac{{\omega_n}^2K+b_1\bullet\dfrac{a_{11}(a_{11}+2\omega_n\zeta)+{\omega_n}^2}{a_{12}}}{a_{11}}-b_2\right)\end{bmatrix}. \tag{19}$$

The feedforward matrix varies with the ideal eigen frequency and the damper coefficient as the feedback matrix.

4.2.3 Steady state gain

The transfer function, which describes the relationship between the yaw rate under steady state and the extra yaw moment, can be obtained from Eq. (6):

$$G^{\dot\psi}_{\Delta M_z}=\frac{(C_f+C_r)V}{(l_f+l_r)^2C_fC_r-mV^2(C_fl_f-C_rl_r)}. \tag{20}$$

Compared with the original system, the extra yaw moment that needs to be added to the controlled system is

$$\Delta M_z=\frac{\Delta\dot\psi}{G^{\dot\psi}_{\Delta M_z}}=\Delta\dot\psi\bullet$$
$$\frac{(l_f+l_r)^2C_fC_r-mV^2(C_fl_f-C_rl_r)}{(C_f+C_r)V}, \tag{21}$$

where $\Delta\dot\psi$ is the differential steady-state yaw rate of the controlled system to the original system and calculated by:

$$\Delta\dot\psi=\delta_f(K-1)\bullet\frac{V/l}{1+kV^2},\ K\in\left[1,1+kV^2\right]. \tag{22}$$

where k is the stability factor of the original vehicle, and

$$k=\frac{m}{l^2}\left(\frac{l_f}{C_r}-\frac{l_r}{C_f}\right).$$

The steady gain K of the controlled system is 1~(1+kV^2) times larger than it was in the original system (if K=1+kV^2, the controlled system becomes neutral steer). K varies with vehicle velocity as shown in Fig. 4(a) because of the stability factor k. So does the required yaw moment deduced from Eqs. (21) and (22) .

In Fig. 4(a), the horizontal line denotes the required yaw moment used to change the original system to a neutral-steer system when velocity varies and lateral acceleration maintains 0.4g. The other three curves show required yaw moment when K equals different multiples of the original at different speeds and with the same lateral acceleration (0.4g). As Fig. 4(a) shows, a larger yaw moment is required with the increase of K.

As a fixed-proportional relation between the yaw rate and the velocity provides drivers coziness, a constant steady gain K that can relieve drivers' effort and keep vehicle stable should be determined. At the working speed of the control system, V=30–80 km/h, the ideal K curve should stay below the neutral steer line or the controlled system would become an oversteering system and be prone to instability. With reference to Fig. 4(a), the ideal steady gain is

$$K_{ideal}=1.04\bullet\frac{V/l}{1+kV^2},$$

The limit of yaw rate $\dot\psi_{\lim}$ is defined as

$$\dot\psi_{\lim}=\frac{a_y}{V}=\frac{0.6\mu g}{V}.$$

And the limit steady gain is

$$K_{\lim}=\frac{\dot\psi_{\lim}}{\delta_f}=\frac{0.6\mu g}{V\delta_f}$$

To ensure the effectiveness of control and keep the vehicle system linear, the real gain under steady state is the smaller value selected from K_{ideal} and $K_{\lim}$, namely

$$K=\min\left\{K_{\text{ideal}},K_{\lim}\right\}=\min\left\{1.04\bullet\frac{V/l}{1+kV^2},\frac{0.6\mu g}{V\delta_f}\right\}.$$

4.2.4 Ideal eigen frequency and damper coefficient

The poles and zeros placement is the purpose of the control system design. The poles and zeros of the controlled system, by Eqs. (13), (17) and (18), are decided by the eigen frequency and the damper coefficient. So an optimal control method is proposed to calculate the ideal eigen frequency and damper coefficient. ITAE is a quality index with good comprehensive dynamic performance and utilized as the objective function of the optimal control.

Control variables ω_n and ζ are subject to the following rules and conditions.

(1) According to stability condition, all poles must be placed in the left half s-plane.

From Eq. (13),

$$-\omega_n\zeta < 0.$$

(2) The system should be small damping or critical damping to ensure the convergence of yaw rate at any vehicle speed. So

$$\zeta \leqslant 1 \quad \text{and} \quad \omega_n > 0.$$

(3) The maximum required yaw moment for control cannot exceed the in-wheel motors' capacity.

As the lower controller is not the emphasis of this paper, a simple rule-based allocation strategy is proposed, namely, the yaw moment obtained by the upper controller is allocated to the front and rear axle averagely and the left and right motor of each axle generate opposite and equal moment.

The required moments of the front axle $T_{rq,f}$ and the rear axle $T_{rq,r}$ can be calculated as follows:

$$\begin{cases} T_{rq,f} = 2T_{\max} \bullet i_a, \\ T_{rq,r} = 2T_{\max} \bullet i_a, \end{cases}$$

where $T_{\max}$ is the maximum output torque of an in-wheel motor, $i_a \in [0,1]$ denotes gas pedal input.

$T_{rq,f}$ and $T_{rq,r}$ are distributed to the left and right in-wheel motors of an axle with the same method. Take the rear axle as an example:

If $T_{rq,r} < T_{r,\max}$, then

$$T_{rl} = \frac{T_{rq,r} - \Delta T_r}{2},\ T_{rr} = \frac{T_{rq,r} + \Delta T_r}{2},$$

where $T_{r,\max}$ is the maximum torque that the rear axle can be generated, ΔT is the differential torque calculated by the upper controller, T_{rl} and T_{rr} are the rear-left and the rear-right in-wheel motor torques respectively.

If $T_{rq,r} > T_{r,\max}$, the in-wheel motor cannot generate enough traction torque while meeting the requirement of the differential torque. And the traction requirement should be satisfied at first. So

$$T_{rl} = T_{\max} - \left(T_{\max} - \frac{T_{rq,r}}{2}\right) - \operatorname{sgn}(\Delta T_r)\left(T_{\max} - \frac{T_{rq,r}}{2}\right),$$

$$T_{rr} = T_{\max} - \left(T_{\max} - \frac{T_{rq,r}}{2}\right) + \operatorname{sgn}(\Delta T_r)\left(T_{\max} - \frac{T_{rq,r}}{2}\right).$$

Characteristics of electrical components of battery or motors are not taken into account. Regenerative braking coefficient equals to 1. Motors that are able to regenerative brake even at low speed have the same external characteristics during drive and brake.

Based on the above allocation strategy, the maximum yaw moment for control generated by the four in-wheel motors of the DDEV is shown in Fig. 4(b), which is another constraint to ω_n and ζ.

To solve the ITAE function within those constraints

$$ITAE = \int_0^{ts} t\left|e(t)\right|\mathrm{d}t,\ \ e = \delta_f \bullet K \bullet \frac{V/l}{1+kV^2} - \dot{\psi}_{act}. \quad (23)$$

It is important to point out that although the variables are only ω_n and ζ, they decide poles directly. And combining with velocity the two variables can determine zeros as well. ω_n and ζ obtained by the optimal control method can place the poles and the zeros simultaneously.

The optimization results at different vehicle velocities are shown in Figs. 4(c) and 4(d).

By substituting the optimization results in Eqs. (15) and (19), the ideal feedback and feedforward matrixes can be obtained.

4.3 Vehicle sideslip angle observer

4.3.1 Sideslip angle observer design

The sideslip angle is a key state variable of the system and it cannot be measured directly. So an observer based on extended Kalman filter was adopted to provide vehicle sideslip angle information to the controller. A diagram block of the observer is shown in Fig. 5. Uncertainty during vehicle run time can be due to tires getting into nonlinear region. In order to ensure the accuracy of the observer within as vast a scale as possible[18] and avoid a large number of floating-point computations led by solving Jacobian matrixes[19], a nonlinear 2DOF vehicle model based on arctangent tire model is built for the observer.

The nonlinear 2DOF vehicle system is described as

$$\begin{cases} \dot{x}_1 = \dfrac{1}{mV}\left\{c_{f1}\operatorname{atan}\left[c_{f2}\left(\delta_f - x_1 - \dfrac{l_f}{V}x_2\right)\right]\cos\delta_f + \right. \\ \qquad \left. c_{r1}\operatorname{atan}\left[c_{r2}\left(-x_1 + \dfrac{l_r}{V}x_2\right)\right]\right\} - x_2, \\ \dot{x}_2 = \dfrac{1}{I_z}\left\{l_f c_{f1}\operatorname{atan}\left[c_{f2}\left(\delta_f - x_1 - \dfrac{l_f}{V}x_2\right)\right]\cos\delta_f - \right. \\ \qquad \left. l_r c_{r1}\operatorname{atan}\left[c_{r2}\left(-x_1 + \dfrac{l_r}{V}x_2\right)\right] + u\right\}. \end{cases} \quad (24)$$

where $x_1 = \beta,\ \ x_2 = \dot{\psi},\ \ u = Mz.$

An extended Kalman filter is based on the traditional Kalman filter, expands the nonlinear function in Taylor series, omits the second order and finishes linearization. The nonlinear Eq. (24), which is estimated by an extended Kalman filter, can be described as

$$\dot{x} = f(x(t),u(t)),\ y = h(x(t),u(t)).$$

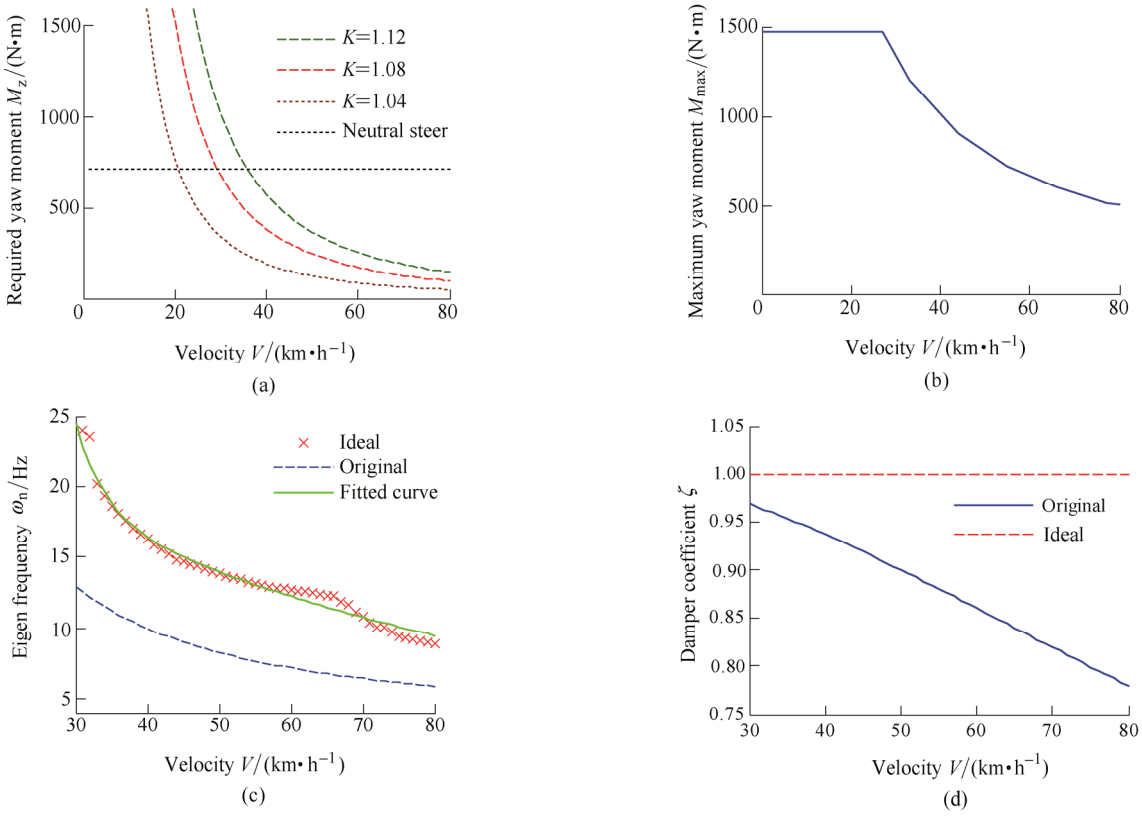

Fig. 4. Main parameters of the control system

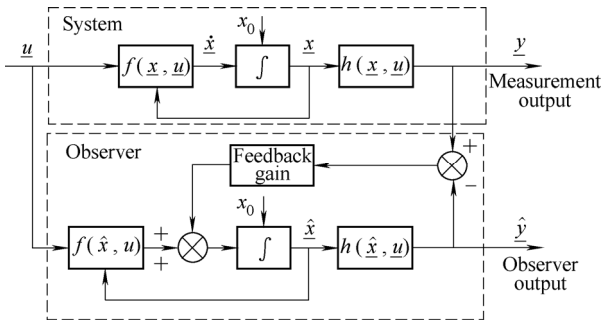

Fig. 5. Diagram block of sideslip angle observer

The Jacobian matrixes are as follows:

$$\frac{\partial f_1}{\partial x_1}=\frac{1}{mv}\left[-\frac{c_{f1}c_{f2}\cos\delta}{1+c_{f2}^2(\delta-x_1-(l_f/v)\cdot x_2)^2}-\frac{c_{r1}c_{r2}}{1+c_{r2}^2(-x_1+(l_r/v)\cdot x_2)^2}\right],$$

$$\frac{\partial f_1}{\partial x_2}=\frac{1}{mv}\left[-\frac{c_{f1}c_{f2}\frac{l_f}{v}\cos\delta}{1+c_{f2}^2\left(\delta-x_1-\frac{l_f}{v}x_2\right)^2}+\frac{c_{r1}c_{r2}\frac{l_r}{v}}{1+c_{r2}^2\left(-x_1+\frac{l_r}{v}x_2\right)^2}\right]-1,$$

$$\frac{\partial f_2}{\partial x_1}=\frac{1}{J}\left[-\frac{l_f c_{f1}c_{f2}\cos\delta}{1+c_{f2}^2(\delta-x_1-(l_f/v)\cdot x_2)^2}+\frac{l_r c_{r1}c_{r2}}{1+c_{r2}^2(-x_1+(l_r/v)\cdot x_2)^2}\right],$$

$$\frac{\partial f_2}{\partial x_2}=\frac{1}{J}\left[-\frac{l_f c_{f1}c_{f2}\cos\delta\frac{l_f}{v}}{1+c_{f2}^2\left(\delta-x_1-\frac{l_f}{v}x_2\right)^2}-\frac{l_r c_{r1}c_{r2}\frac{l_r}{v}}{1+c_{r2}^2\left(-x_1+\frac{l_r}{v}x_2\right)^2}\right],$$

$$\frac{\partial h}{\partial x_1}=0,\quad \frac{\partial h}{\partial x_2}=1.$$

After linearization, the system can be estimated using a traditional Kalman filter approach.

4.3.2 *Sideslip angle observer validation*

The precision of the sideslip angle observer was validated through simulations in Carsim®. The vehicle configuration in Carsim® is set according to Table 1. Simulation condition: Double-lane change test with vehicle velocity at 40 km/h and tire-road friction coefficient μ=1.0.

The results in Fig. 6 indicate that the observer had satisfactory accuracy when the lateral acceleration was less than $0.6\,\mu g$, namely, under normal driving conditions.

For the sideslip angle observer, more details and multiple validations studied by the author's team can be found in Ref. [20].

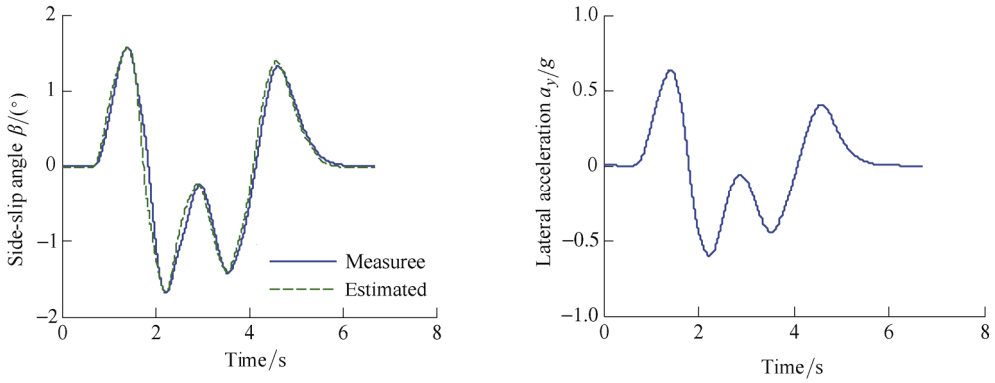

Fig. 6. Results of double-lane change test

5 Simulation Results of the Control System

To check the performance of the proposed control system, simulations were carried out based on a Carsim® and MATLAB/Simulink joint simulation platform. The vehicle configuration in Carsim® was set according to Table 1. A simplified magic formula tire model was obtained by fitting tire test data.

5.1 Steering wheel angle step input test

Transient and steady-state responses of this test indicate time-domain response of vehicle handling stability. In simulations, vehicle velocity was 50 km/h and constant; road friction coefficient was 1.0, and steering wheel turned 60° in 0.2 s. Simulation results are shown in Fig. 7.

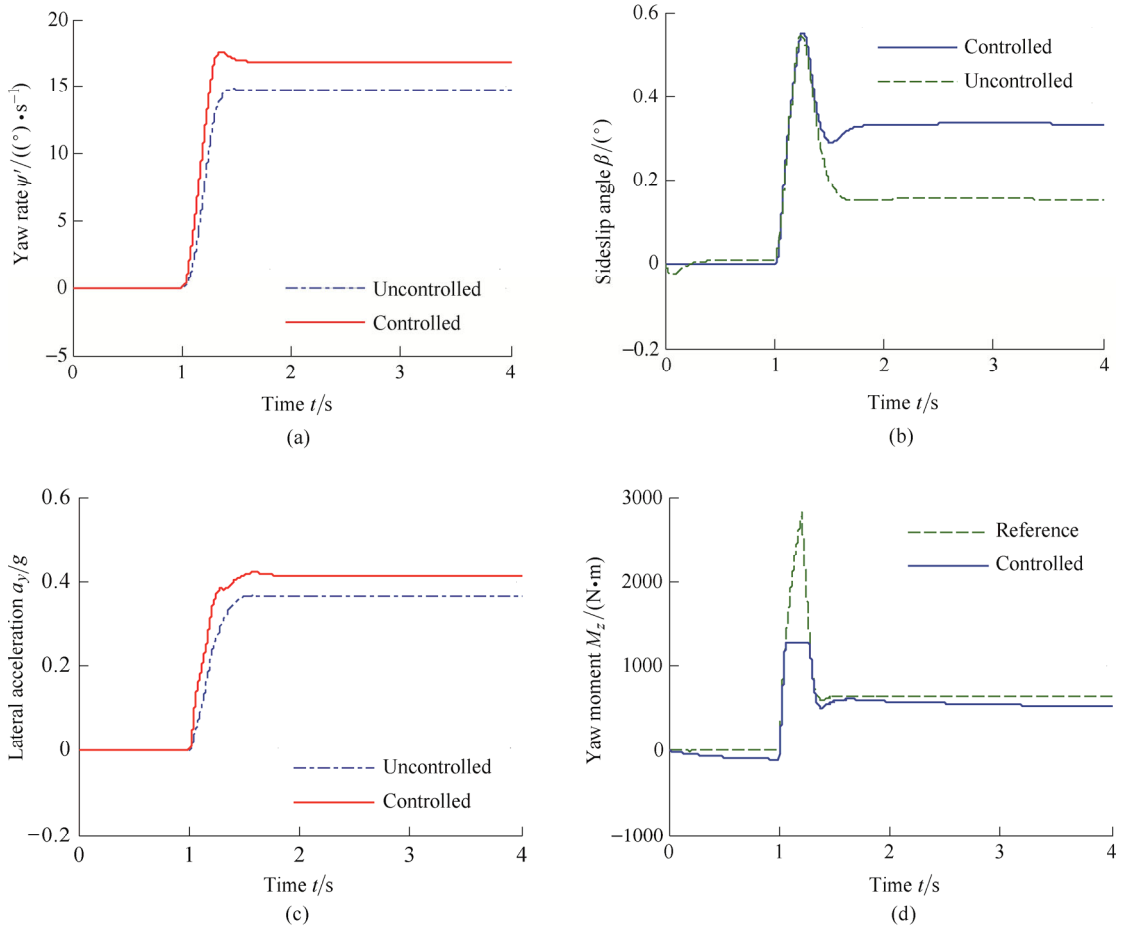

Fig. 7. Simulation results in steering wheel angle step input test

As shown in Fig. 7(a), it took about 0.5 s for the uncontrolled vehicle to raise the yaw rate from zero to peak but only 0.3 s for the controlled vehicle, which means improvement in transient response. The overshoot of the controlled system was 2.8% while 0.3% in the uncontrolled system, but still remained within the engineering permission scope.

5.2 Steady state turning test

The purpose of this test is to obtain steady-state yaw rate response and vehicle steer characteristics. Operator kept steering wheel angle at 60°, accelerated vehicle uniformly and continuously with the longitudinal acceleration less than 0.25 m/s^2 until the lateral acceleration was raised to 6.5 m/s^2. Tire-road friction coefficient was 1.0. Simulation results are shown in Fig. 8.

Fig. 8(a) shows obviously that the yaw rate curve in the controlled system raises faster than in the uncontrolled system, which means the decrease of understeer characteristics and the increase of yaw-rate steady-state gain. Drivers' burdens are reduced.

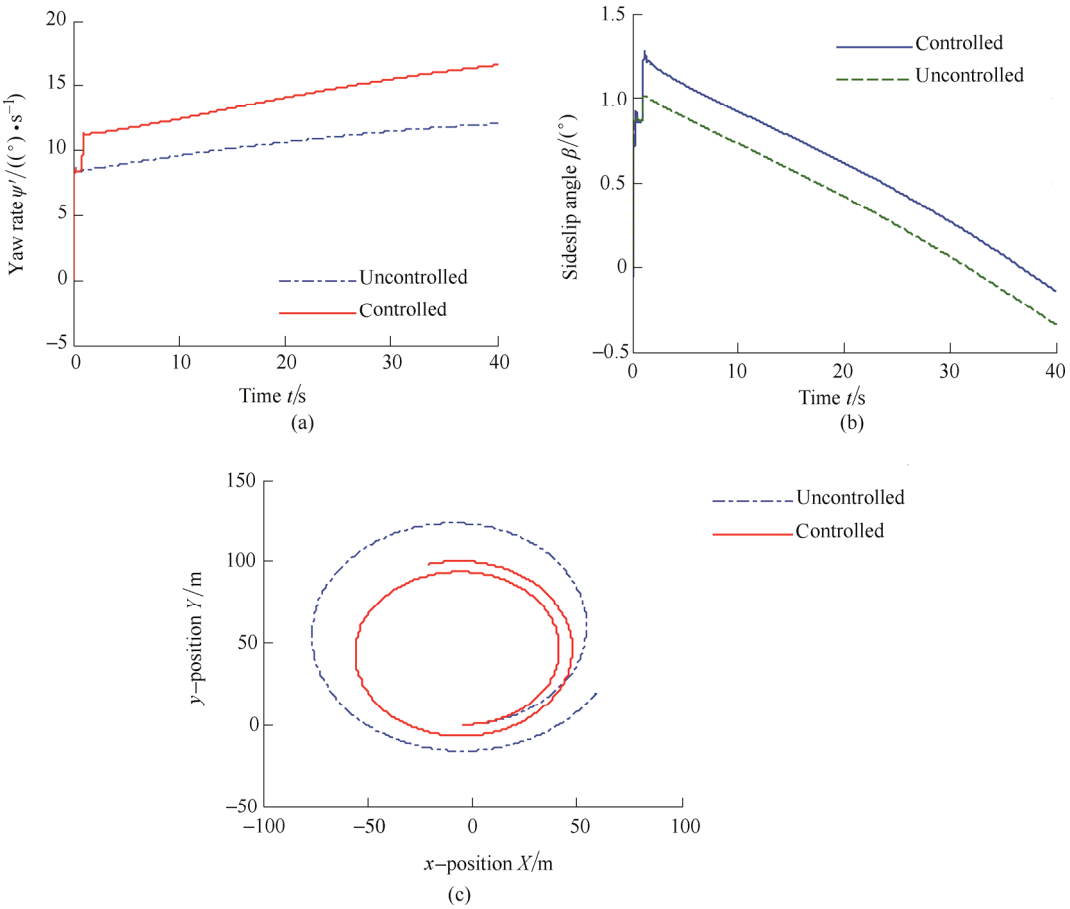

Fig. 8. Simulation results in steady state turning test

6 Experimental Results of Control System

6.1 Slalom test

Slalom tests were designed with a reference to Chinese National Standard for vehicle handling and stability test procedure (GB/T 6323-1994[21]). The horizontal distance between two cones in the slalom experiment was set 12 m because of space and vehicle limitations. Velocity was kept around 35 km/h; tire-road friction coefficient was 0.85. Experiment results are shown in Fig. 9.

Thanks to the control system, the steering wheel angle was decreased by 93°, from 343° to 250° (absolute values), reducing handling burdens dramatically as shown in Fig. 9(b). Comparing steering wheel angle in the process of counter clockwise rotation with control, the peak values were all reduced, especially in the latter half of the test, which means the controlled vehicle had better path tracking ability. Table 2 shows comparison results of steering wheel angle in different systems regardless of the first and the last cones.

Table 2. Comparison of steering wheel angle

No.	Steering wheel angle (°)		Change rate (%)
	Without control	With control	
Cone 2	161	142	–11.80
Cone 3	170	213	25.29
Cone 4	343	250	–27.11
Cone 5	215	205	–4.65
Cone 6	298	248	–16.78
Cone 7	225	201	–10.67

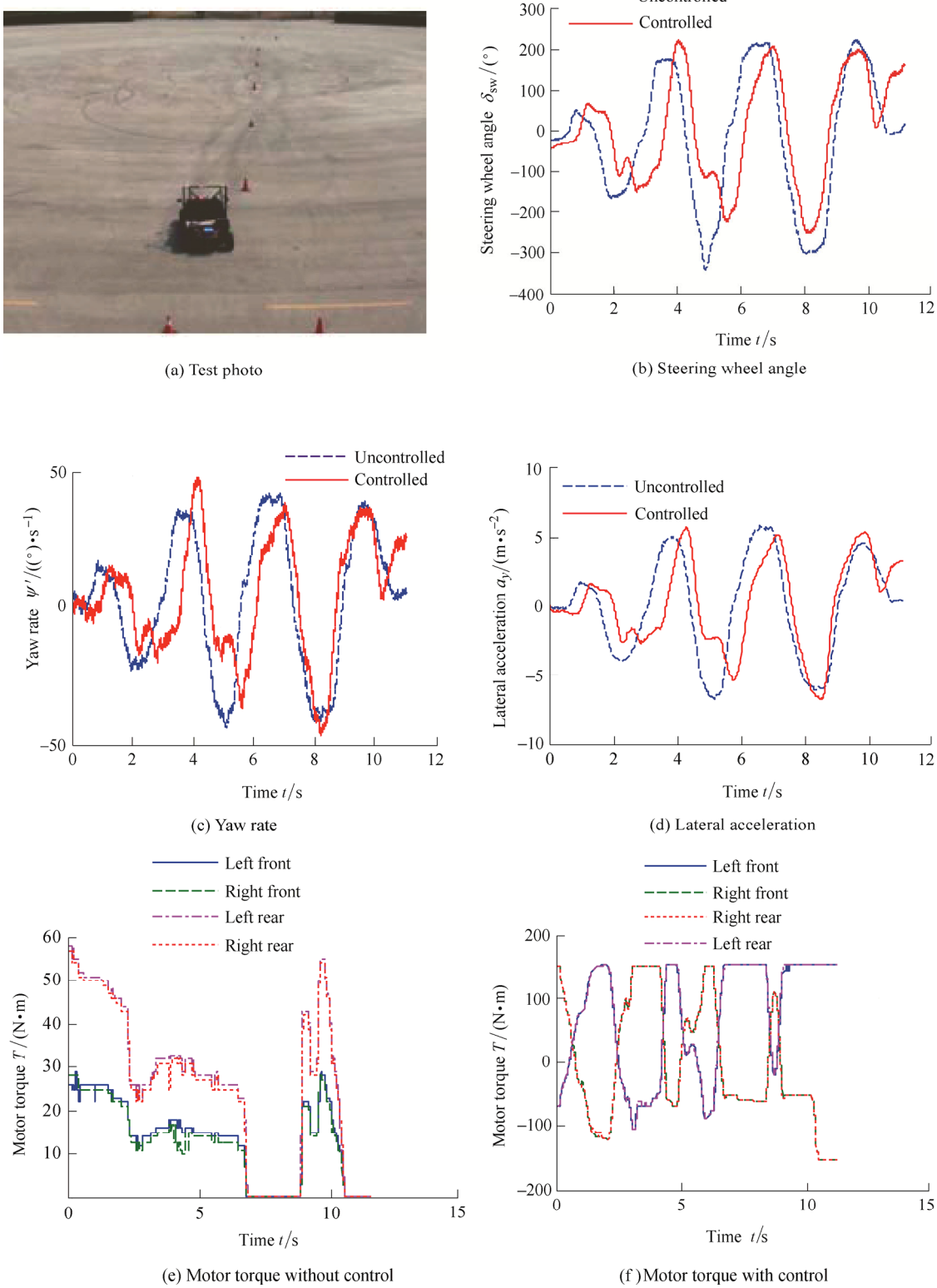

(a) Test photo

(b) Steering wheel angle

(c) Yaw rate

(d) Lateral acceleration

(e) Motor torque without control

(f) Motor torque with control

Fig. 9. Experiment results of the slalom test

6.2 Obstacle avoidance test

Obstacle avoidance test, which is a typical test for vehicle close-loop maneuverability and stability, was designed with a reference to ISO 3888-2:2002[22]. Vehicle velocity was kept about 40 km/h to 50 km/h; tire-road friction coefficient was 0.85. The experiment results of the obstacle avoidance test are shown in Fig. 10.

Table 3 shows a detailed comparison of the steering wheel angle results. The proposed controller reduced steering wheel angles and eased handling burdens.

Table 3. Comparison of steering wheel angle

Position	Steering wheel angle (°)		Change rate (%)
	Without control	with control	
First peak	79	56	–29.11
Second peak	180	122	–32.22
Third peak	131	60	–54.20

(a) Test photo

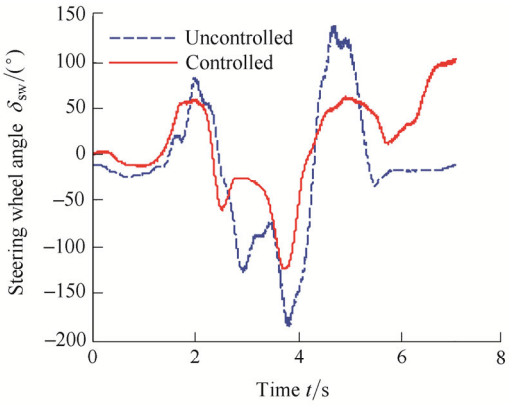

(b) Steering wheel angle

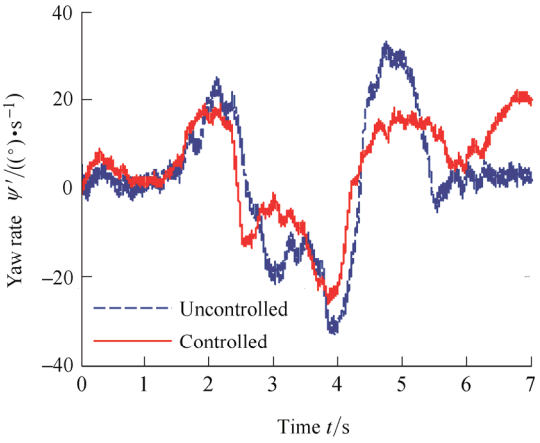

(c) Yaw rate

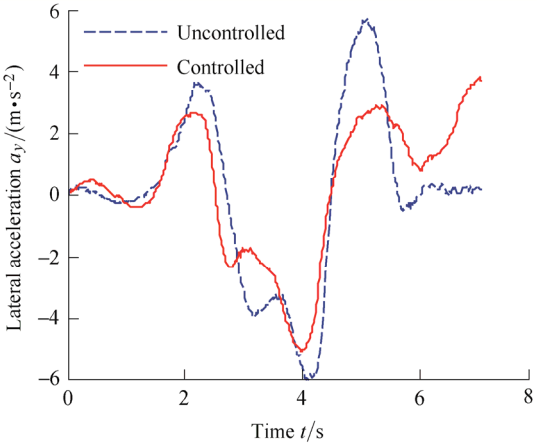

(d) Lateral acceleration

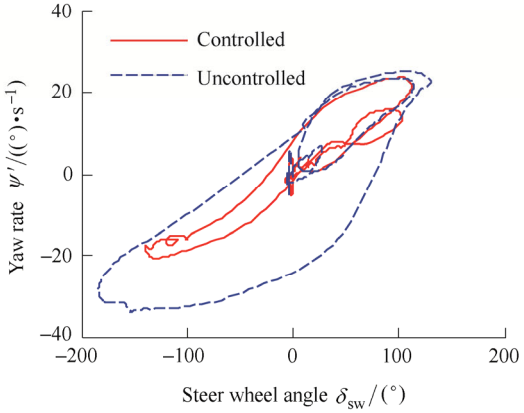

(e) Hysteresis curve

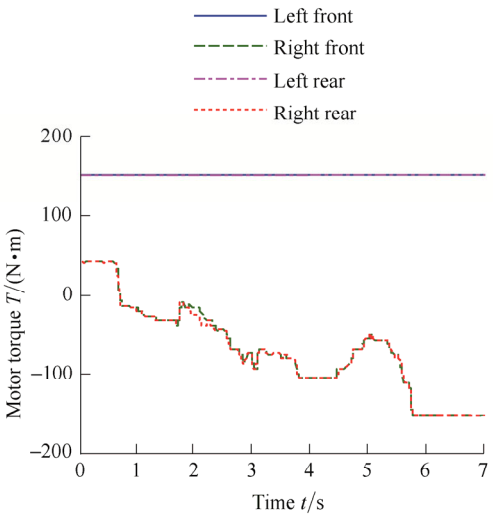

(f) Motor torque with control

Fig. 10. Experiment results of obstacle avoidance

Fig. 10(e) shows hysteresis curves of steer wheel angle and yaw rate with and without control. With the proposed control method, the response delay of yaw rate to steer wheel angle input decreased. And the relation of yaw rate and steer wheel angle tended to be linear. Namely, the vehicle was close to neutral steer.

7 Conclusions

In this paper, a handling improvement control system based on direct yaw moment control for a distributed drive electric vehicle equipped with four in-wheel motors was presented under normal driving conditions.

The designed controller consists of a state feedback controller and a steering wheel angle feedforward controller. The state feedback based control system, which is different from the model following control widely used in previous research, can reduce modeling difficulty and regulate zeros and poles of the system simultaneously. An observer based on extended Kalman filter and nonlinear two degree of

freedom vehicle model was adopted to provide vehicle sideslip angle information to the controller.

The ITAE function was utilized as the objective function in the optimal control with the consideration of motor capacity to calculate the ideal eigen frequency and damper coefficient of the system. Optimal feedback matrix and feedforward matrix were obtained.

Simulations were carried out based on a Carsim and MATLAB/Simulink co-simulation platform to test the performance of the control system. Simulation results indicated that the yaw rate responded faster, the yaw rate rise time was reduced by 40%. The steady-state yaw rate gain increased nearly 20% leading to an approximately neutral steer, which also reduced handling burdens.

Finally, two typical closed-loop experiments, the slalom test and the obstacle avoidance test, were carried out based on a high performance DDEV for evaluating vehicle handling performance. In the slalom tests, the peak steering wheel angle was decreased by 93°, the change rate was more than 27%. Obstacle avoidance tests results showed that the vehicle with control was easier to handle, which not only reduced drivers burdens but was significant to vehicle active safety. The experiments results validated the precision and the practicability of the designed control system.

References

[1] SHIBAHATA Y, SHIMADA K, TOMARI T. Improvement of vehicle maneuverability by direct yaw moment control[J]. *Vehicle System Dynamics*, 1993, 22(516): 465–481.

[2] YANG P, XIONG L, YU Z, et al. Motor/hydraulic systems combined stability control strategy for distributed electric drive vehicle[C]//*AVEC'14 12th International Symposium on Advanced Vehicle Control*, Tokyo, Japan, September 22–26, 2014: 421–424.

[3] HORI Y. Future vehicle driven by electricity and control-research on four-wheel-motored" UOT Electric March II"[J]. *Industrial Electronics, IEEE Transactions on*, 2004, 51(5): 954–962.

[4] YU Z, FENG Y, XIONG L. Review on vehicle dynamics control of distributed drive electric vehicle[J]. *Journal of Mechanical Engineering*, 2013, 49(8): 105–114. (in Chinese)

[5] IKUSHIMA, SAWASE: A study on the effect of active yaw moment control[G]. *SAE Paper 950303*, 1995.

[6] ONO E, HATTORI Y, MURAGISHI Y, et al. Vehicle dynamics integrated control for four-wheel-distributed steering and four-wheel-distributed traction/braking systems[J]. *Vehicle System Dynamics*, 2006, 44(2): 139–151.

[7] SHINO M, NAGAI M. Independent wheel torque control of small-scale electric vehicle for handling and stability improvement[J]. *JSAE Review*, 2003, 24(4): 449–456.

[8] KIM J, PARK C, HWANG S, et al. Control algorithm for an independent motor-drive vehicle[J]. *IEEE Transactions on Vehicular Technology*, 2010, 59(7): 3213–3222.

[9] XIONG L, YU Z, WANG Y, et al. Vehicle dynamics control of four in-wheel motor drive electric vehicle using gain scheduling based on tyre cornering stiffness estimation[J]. *Vehicle System Dynamics*, 2012, 50(6): 831–846.

[10] HE P, HORI Y. Optimum traction force distribution for stability improvement of 4WD EV in critical driving condition[C]//*9th IEEE International Workshop on Advanced Motion Control*, Istanbul, Turkey, 2006: 596–601.

[11] SHINO M, NAGAI M. Yaw-moment control of electric vehicle for improving handling and stability[J]. *JSAE Review*, 2001, 22(4): 473–480.

[12] SHINO M, NAGAI M. Independent wheel torque control of small-scale electric vehicle for handling and stability improvement[J]. *JSAE Review*, 2003, 24(4): 449–456.

[13] KIM D, KIM C, KIM S, et al. Development of adaptive direct yaw-moment control method for electric vehicle based on identification of yaw-rate model[C]//*2011 IEEE Intelligent Vehicles Symposium (IV)*, Baden-Baden, Germany, June 5–9, 2011: 1098–1103.

[14] MITSCHKE M, WALLENTOWITZ H. *Dynamik der Kraftfahrzeuge*[M]. Berlin: Springer, 2003.

[15] DORF R, BISHOP R. *Modern control systems*[M]. 11th ed. Beijing: Pearson, 2011.

[16] FENG Y, YU Z, XIONG L, et al. Torque vectoring control for distributed drive electric vehicle based on state variable feedback[C]//*SAE 2014 World Congress and Exhibition*, Detroit, USA, April 8–10, 2014: SAE Paper 2014-01-0155.

[17] AWOUDA A, MAMAT R. New PID tuning rule using ITAE criteria[J]. *International Journal of Engineering*, 2010, 3(6): 597–608.

[18] GUO K, FU H, DING H. Estimation of CG sideslip angle based on extended Kalman filter[J]. *Automobile Technology*, 2009(4): 1–3, 44. (in Chinese)

[19] HIEMER M. *Model based detection and reconstruction of road traffic accidents*[M]. Karlsruhe: Universitätsverlag Karlsruhe, 2004.

[20] GAO X, YU Z, NEUBECK J, et al. Sideslip angle estimation based on input-output linearization with tire-road friction adaptation[J]. *Vehicle System Dynamics*, 2010, 48(2): 217–234.

[21] GB/T 6323-1994. *Controllability and stability test procedure for automobile*[S]. Beijing: Standardization Administration of the People's Republic of China, 1994. (in Chinese)

[22] ISO 3888-2:2002. *Passenger cars-Test track for severe lane-change maneuver-Part 2: Obstacle avoidance*[S]. London: British Standards Institution, 2003.

Biographical notes

YU Zhuoping, born in 1960, is currently a professor at *School of Automotive Studies, Tongji University, China*. His research interests include vehicle dynamics and control, intelligent vehicle and parameter estimation.
Tel: +86-21-69589119; E-mail: yuzhuoping@tongji.edu.cn

LENG Bo, born in 1991, is currently a PhD candidate at *School of Automotive Studies, Tongji University, China*. He received his bachelor degree from *Tongji University, China*, in 2014. His research interests include vehicle dynamics and control.
Tel: +86-21-69589124; E-mail: harrisonleng@gmail.com

XIONG Lu, born in 1978, is currently an associate professor at *School of Automotive Studies, Tongji University, China*. His research interests include vehicle dynamics and control, unmanned ground vehicle motion control and chassis system design and development.
Tel: +86-21-69589124; E-mail: xiong_lu@tongji.edu.cn

FENG Yuan, born in 1987, received his doctor degree from *Tongji University, China*, in 2015. His research interests include vehicle dynamics and control, parameter estimation.
E-mail: ryan_fengyuan@163.com

SHI Fenmiao, born in 1988, received her master degree from *Tongji University, China*, in 2014. Her research interests include vehicle dynamics and control.
E-mail: juliannesl@163.com